Developmental Cell
Article

FHOD1 Is Needed for Directed Forces and Adhesion Maturation during Cell Spreading and Migration

Thomas Iskratsch,[1,*] Cheng-Han Yu,[2] Anurag Mathur,[3,5] Shuaimin Liu,[3] Virginie Stévenin,[1] Joseph Dwyer,[4] James Hone,[3] Elisabeth Ehler,[4] and Michael Sheetz[1,2,*]
[1]Department of Biological Sciences, Columbia University, New York, NY 10027, USA
[2]Mechanobiology Institute, National University of Singapore, Singapore 117411, Singapore
[3]Department of Mechanical Engineering, Columbia University, New York, NY 10027, USA
[4]Randall Division of Cell and Molecular Biophysics and Cardiovascular Division, King's College London, London SE1 1UL, UK
[5]Present address: Department of Bioengineering and California Institute for Quantitative Biosciences (QB3), University of California at Berkeley, Berkeley, CA 94720, USA
*Correspondence: ti2170@columbia.edu (T.I.), ms2001@columbia.edu (M.S.)
http://dx.doi.org/10.1016/j.devcel.2013.11.003

SUMMARY

Matrix adhesions provide critical signals for cell growth or differentiation. They form through a number of distinct steps that follow integrin binding to matrix ligands. In an early step, integrins form clusters that support actin polymerization by an unknown mechanism. This raises the question of how actin polymerization occurs at the integrin clusters. We report here that a major formin in mouse fibroblasts, FHOD1, is recruited to integrin clusters, resulting in actin assembly. Using cell-spreading assays on lipid bilayers, solid substrates, and high-resolution force-sensing pillar arrays, we find that knockdown of FHOD1 impairs spreading, coordinated application of adhesive force, and adhesion maturation. Finally, we show that targeting of FHOD1 to the integrin sites depends on the direct interaction with Src family kinases and is upstream of the activation by Rho kinase. Thus, our findings provide insights into the mechanisms of cell migration with implications for development and disease.

INTRODUCTION

The events following fibroblast binding to and spreading on matrix-coated surfaces can be described by a series of sequential steps (Dubin-Thaler et al., 2008). The earliest events involve the clustering of the integrins to activate adhesion (Jiang et al., 2003). On solid substrates, integrin activation results in rapid spreading and adhesions mature over time through the contraction process (Cai et al., 2010; Giannone et al., 2004). In suspension cells, the binding of soluble ligand to integrins causes activation of Src family kinases (SFKs; Huveneers and Danen, 2009), but the process stalls because subsequent steps involve or depend on surface forces. Recent studies of arginine-glycine-aspartic acid (RGD) ligands attached to mobile lipids with or without barriers to movement show that the initiation of spreading follows actin polymerization from clustered integrins, subsequent recruitment of myosin, and force generation on the clusters (Yu et al., 2011). Actomyosin contractions of integrin clusters to the barriers are important to trigger further spreading by the previously reported pathways (Giannone et al., 2004). This raises the question of how actin polymerization occurs at the integrin clusters and whether it is downstream of SFKs. Since actin filament attachment to RGD-integrin clusters is critical for subsequent steps in the spreading process, we focus here on elucidating the mechanism of actin polymerization following integrin activation.

The ARP2/3 complex (Goley and Welch, 2006; Lai et al., 2008; Svitkina and Borisy, 1999) and several formins are detected in fibroblasts and associate with a range of actin structures, such as filopodia or stress fibers (Campellone and Welch, 2010; Mellor, 2010). Although the function of the ARP2/3 complex was closely linked to cell spreading, knockdown experiments or the use of specific ARP2/3 inhibitors indicate that additional actin assembly factors are involved in spreading (Di Nardo et al., 2005; Nolen et al., 2009; Steffen et al., 2006). In a screening of fibroblast actin assembly factors, we found localization of FHOD1 to early RGD clusters, whereas other prominent fibroblast formins such as mDia1, mDia2, or FMNL3 were not targeted to the integrin sites. Indeed, FHOD1 is an interesting candidate for actin assembly from early integrin sites as it is (1) regulated downstream of SFKs (Koka et al., 2005), even though details of the interaction remained unclear, and (2) FHOD1 has both a barbed end elongation activity and a strong actin bundling activity (Schönichen et al., 2013). Although in mature adhesions actin filaments are bundled by α-actinin and other actin crosslinking proteins to ensure optimal force transmission (Roca-Cusachs et al., 2012, 2013), a combined elongation and bundling activity could guide assembly of contractile structures in the context of early integrin cluster formation.

To analyze a potential role of FHOD1 during early cell spreading, we combined spreading assays on supported lipid bilayers and on rigid substrates, as well as on high-precision force-measuring pillar arrays. Whereas spreading assays on rigid substrates are a well-established model for cell motility,

the supported lipid bilayers provide an important contrast because they conserve steps of cell adhesion and spreading that occur prior to myosin contraction (Yu et al., 2011). Combining these methods, we provide evidence that FHOD1 is active at early integrin clusters that support actin polymerization. Furthermore, the knockdown of FHOD1 causes an actin assembly defect from early adhesion sites and inhibits cell spreading through alterations in inward traction stress and adhesion maturation. Finally, we find that the interaction between SFKs and FHOD1 is needed for adhesion targeting and subsequent activation.

RESULTS

FHOD1 Targets to Early Integrin Clusters

In order to investigate a potential association of FHOD1 with early adhesions, we employed supported lipid membranes functionalized with RGD peptides as the ligand for integrins. Two-dimensional (2D) mobility of the ligand on supported membranes enabled us to visualize the reorganization of activated integrins and the newly formed actin network associated with integrin clusters in live cells (Yu et al., 2011). FHOD1 is a low-abundance protein, and transfection resulted in a strong overexpression (Figure S1A available online). Therefore, we focused on the analysis of low to moderately overexpressing cells. As cells started to adhere, fluorescently labeled RGD on supported bilayers formed submicron clusters. As soon as clusters were visible, ribbon-like polymerization of actin and FHOD1 binding were observed at RGD-integrin clusters (Figures 1A and 1B; Movie S1). As the clusters grew in size, the actin ribbons extended away (Figures 1B and 1C, red arrowheads). The FHOD1 signal was more intense closer to the centers of the clusters (Figure 1B, green arrowheads; Figure 1C, blue asterisks), but partially moving outward with the actin as well (Figure 1C, red arrowheads). An enrichment of both FHOD1 and actin around RGD clusters was confirmed by plotting the averaged radial profiles of cells spread for 5 min (Figures 1D and 1E). This behavior was specific for FHOD1, as other major fibroblast formins, such as mDia1, mDia2, or FMNL3, were not targeted to the clusters and localized diffusely to the cytoplasm (Figure S2).

To exclude that this localization was an artifact of the lipid bilayer system, we next analyzed FHOD1's localization during cell spreading on fibronectin-coated coverslips. Cell spreading on rigid 2D surfaces was previously characterized by a phasic response that includes initial contact formation (or P0 phase), a fast increase in cell area driven by actin polymerization (P1), and periodic actomyosin contractions that propagate along the edge in lateral waves (P2) (Döbereiner et al., 2006; Dubin-Thaler et al., 2008; Giannone et al., 2007). The latter phase also includes the formation of early integrin adhesions along the cell edge, which mature over time. In our experiments, FHOD1-GFP showed a dynamic localization to actin structures in spreading fibroblasts during the P1 and P2 phase. The maximum intensity of the FHOD1 signal was observed behind the protruding cell edge (Figure 2A; Movie S2), close to the site of the lamellipodium-lamella interface. Additionally, in some instances FHOD1-GFP speckles appeared to be closer to the cell edge and inside the lamellipodium (see Figure 2B for kymograph and Figure 2C for image sequence). FHOD1 aggregates grew in size over time before disappearing again as the cell protruded further. Such behavior was reminiscent of the formation of nascent adhesions in the lamellipodium, as well as their maturation at the boundary between lamellum and lamellipodium (Alexandrova et al., 2008). Indeed cotransfection with paxillin showed partial colocalization at nascent and mature focal adhesions (Figure 2D).

Since the lipid bilayer experiments suggested that localization of FHOD1 to integrin clusters was independent of myosin-generated forces, we next analyzed the localization of FHOD1 in cells that were pretreated with and spread in the presence of blebbistatin. As reported previously (Choi et al., 2008), blebbistatin inhibited adhesion maturation and paxillin was found in nascent adhesions around the cell edge (Figure 2E). There, FHOD1 colocalized with paxillin, supporting the model that FHOD1 localization is independent of myosin II. In contrast, this localization was dependent on integrin activation by surface antigens, since no localization close to the cell edge was found when the cells were spread on poly-L-lysine (Figure 2F). Immunostaining with an anti-FHOD1 antibody confirmed the localization pattern to the tips of radial actin filaments (Figures 2G and S1A). Interestingly, both transfected as well as endogenous FHOD1 were at least partially detected in a periodic pattern along the actin filaments, which could be related to an actin bundling activity (Schönichen et al., 2013).

We next sought to analyze whether FHOD1 was active during early cell spreading and, thus, could be involved in actin assembly at the early integrin clusters and adhesions. Formins of the FHOD subfamily are known to be activated by phosphorylation of a consensus sequence in the diaphanous autoregulatory domain by Rho kinase (ROCK), which results in the release of the auto-interaction and promotion of actin assembly (Iskratsch et al., 2013; Takeya et al., 2008). Using a phosphospecific antibody (Figures 2H and S1C–S1E), we found the peak of FHOD1 activity 3–8 min after cell plating, and thus at times where the majority of cells started to form adhesions at the cell edge.

FHOD1 Knockdown Inhibits Cell Spreading

To further test whether FHOD1 was required during early cell spreading for the actin assembly from adhesion sites, we designed small hairpin RNA (shRNA) constructs against FHOD1 (Figure S1B). FHOD1 knockdown cells formed filopodia, but failed to form coherent protrusions and spread in a segmented fashion (Figure 3A; Movies S3 and S4). Frequently, protrusions were not stable and collapsed entirely (arrows in Figure 3A). Moreover, the speed of cell spreading was strongly reduced (Figure 3B). Cell area, shape, and F-actin content were restored to normal levels by coexpression of small interfering RNA-resistant (siRNA-resistant) human FHOD1 (Figure S3). Similarly, treatment with the pan-formin inhibitor smiFH2 impaired cell spreading in a dose-dependent manner (Figure S4), thus confirming the requirement for formin family proteins for early cell spreading.

FHOD1 Knockdown Suppresses Focal Adhesion Formation

Since FHOD1 localized to early adhesions and protrusions in knockdown cells were less stable, we tested whether there was a defect in focal adhesion formation. For this we knocked

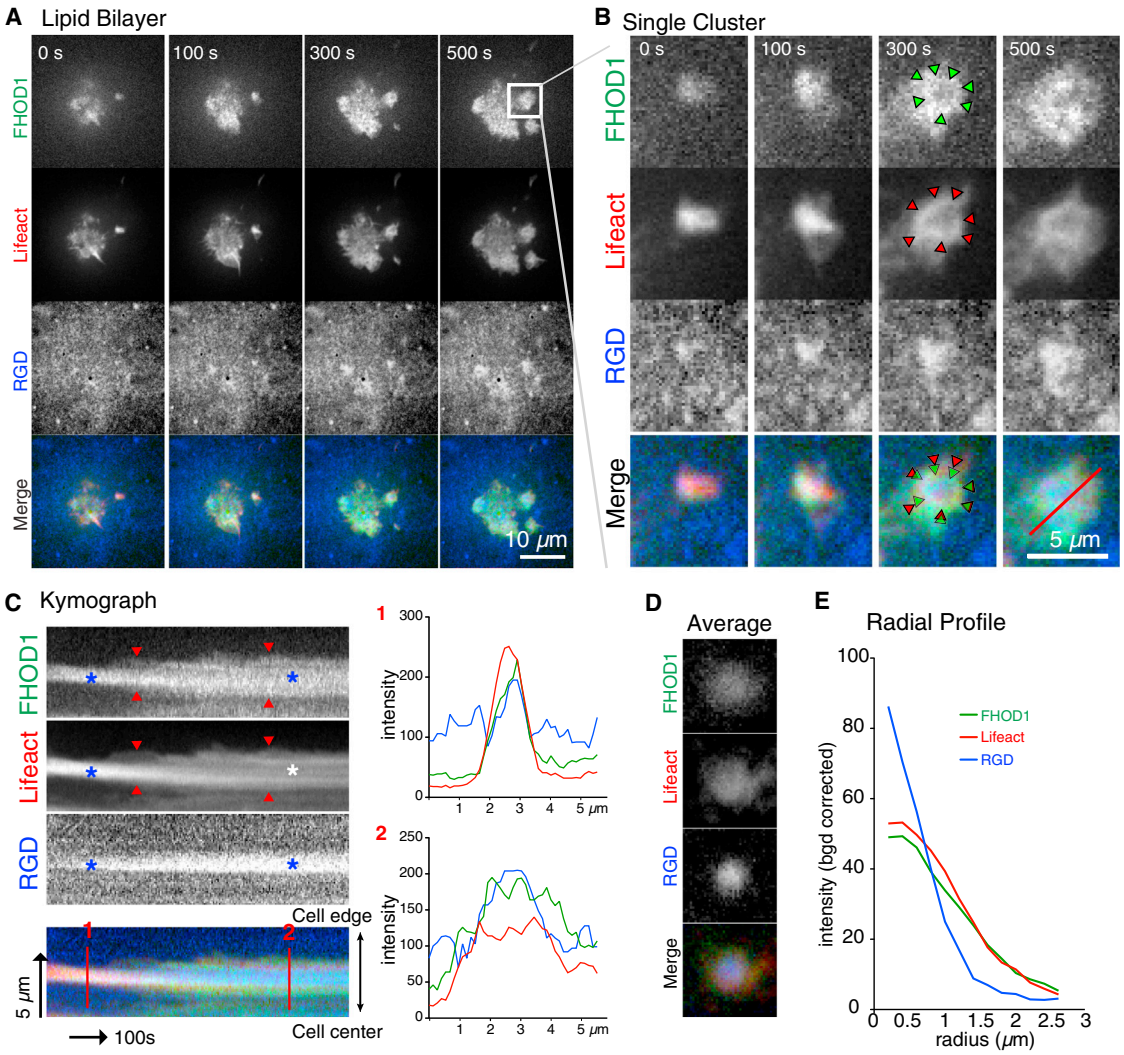

Figure 1. FHOD1 Localizes to Early Integrin Clusters

(A) MEF cells were transiently transfected with Ruby-Lifeact and GFP-FHOD1 and then plated onto RGD membrane labeled with Cascade Blue neutravidin. Ribbon-like actin polymerizes from RGD clusters and expands outward. FHOD1 is also enriched at RGD clusters.

(B) Zoom of marked area in (A). Red arrowheads indicate actin ribbon and green arrowheads indicate the intensity maxima of FHOD1-GFP.

(C) A kymograph of the region marked by the red line in (B) shows early colocalization of both FHOD1 and Lifeact with the RGD clusters (see line profile 1). At later time points, Lifeact is localized stronger to the periphery of the cluster, and FHOD1 localizes to the center and the periphery of the cluster (line profile 2). Red arrowheads indicate the outward extending actin and FHOD1; blue asterisks indicate the RGD cluster and the colocalizing FHOD1 and actin; white asterisks indicate the center of the cluster that is depleted from actin.

(D and E) RGD clusters of cells spread for 5 min were stacked and averaged with ImageJ. To analyze the enrichment around the clusters, the average pixel intensity outside a circular ROI (radius = 2.5 μm) was subtracted (D) and the radial profile was calculated for each channel (E). n = 31 RGD clusters of seven cells; for mDia1, mDia2, and FMNL3 localization, see Figure S2.

down FHOD1 for 72 hr and then additionally transfected the cells with paxillin-GFP and pRuby-Lifeact and imaged the cells for >20 min, starting with the fast spreading phase (P1) to observe the adhesion formation during the protrusion-retraction phase. During the outward spreading, control cells formed nascent adhesions, many of which matured to focal adhesions after the transition to the protrusion-retraction phase (Figures 3C and 3D; Movie S5). Again, FHOD1 knockdown cells formed protrusions that frequently collapsed. Although knockdown cells initially formed nascent adhesions as well, they did not mature and eventually turned over (see kymograph in Figure 3D). Additionally, the actin filament density and organization was reduced in knockdown cells (Figures 3C, S5A, and S5B). We further confirmed a defect in adhesion formation by immunostaining with an anti-paxillin antibody (Figure 3E). Quantification of the adhesion area showed a significant reduction in FHOD1 knockdown cells and a concomitant increase in the fraction of nascent adhesions (Figures 3F and 3G). Again, treatment with the pan-formin inhibitor showed a similar reduction in adhesion size and F-actin density (Figure S5C). Immunostaining for active β1-integrin (9EG7) showed that the FHOD1 knockdown did not affect the integrin activation at the cell edge, suggesting that

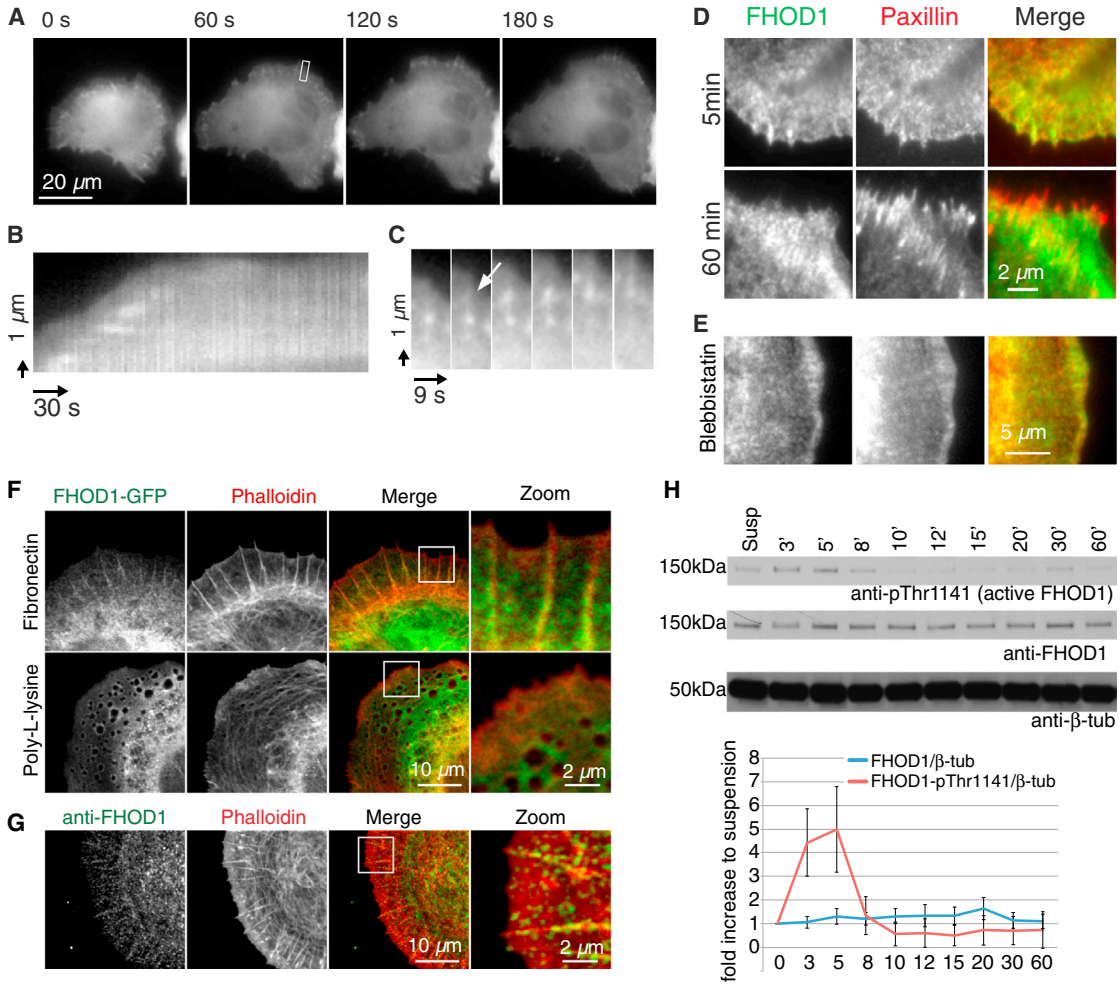

Figure 2. Active FHOD1 Localizes to Adhesions on Fibronectin-Coated Rigid Substrates

(A) MEF cells were transfected with FHOD1-GFP and cells were imaged on a TIRF microscope.

(B) Kymograph of the marked area in (A).

(C) Time series of the marked area in (A).

(D) Cotransfection with paxillin-dsRed shows colocalization at early time points (5 min) and localization of FHOD1 close to adhesions at 60 min.

(E) FHOD1 colocalizes with paxillin also in the absence of myosin II forces (blebbistatin).

(F) Localization to the cell edge is lost when cells are plated on poly-L-lysine.

(G) The targeting pattern could be confirmed by immunostaining with an anti-FHOD1 antibody.

(H) FHOD1 activity was tested by western blotting with the phosphospecific anti-FHOD1 pThr1141 antibody that recognizes the active form. Bands were quantified with ImageJ. n = 3; error bars indicate SD.

See Figure S1 for antibody validation.

FHOD1 acted downstream of integrin engagement (Figure 3H). However, both total and active β1-integrin signals were limited to the cell edge, further documenting the defect in adhesion maturation.

FHOD1 Knockdown Impairs Cell Migration

Cell spreading assays are commonly used as model system for motility experiments and especially for adhesion formation. The highly reproducible sequence of functional phases had in the past led to many important insights (Döbereiner et al., 2006; Dubin-Thaler et al., 2008; Giannone et al., 2004, 2007). Nevertheless, to confirm that FHOD1's role in adhesion formation had a broader relevance for cell migration, we performed wound scratch assays in control and FHOD1 knockdown cells (Figures 3I–3L). After application of a wound with a pipette tip, control cells started to migrate quickly toward the center of the wound and the wound was closed within approximately 24 hr. FHOD1 knockdown cells, in contrast, migrated slowly and only one-third of the wound was closed within 24 hr (Figures 3J and 3K). When we fixed the cells after 8 hr, we found that, similar to the spreading assays, FHOD1 knockdown cells lacked strong, polarized actin filaments and adhesions were frequently limited to the periphery and had a dot-like appearance (Figure 3L). Within the first 50 μm from the leading edge (i.e., approximately the first row of cells), the cell area occupied by adhesions was reduced from 17.0% ± 1.3 to 6.7% ± 0.4

(n = 14 images with approximately five cells each from three experiments; $p < 0.0001$). This suggested that impaired adhesion formation was a general characteristic of FHOD1 knockdown cells that contributes to spreading, as well as migration defects (Figure 3L).

FHOD1 Is Necessary for Effective Force Transmission at Integrin Adhesions

The lack of adhesion maturation suggested a potential defect in the force coupling at the adhesion. Therefore, we plated cells on sub-micron polydimethylsiloxane (PDMS) pillar arrays that enabled nondisruptive live imaging of localized traction forces (Ghassemi et al., 2012). Surprisingly, there was a complete lack of coordinated inward forces in knockdown cells. Whereas in control cells whole rows of pillars were displaced perpendicular to the cell edge over tens of seconds, pillar displacement magnitude and angles fluctuated wildly in knockdown cells (Figures 4A–4C; Movie S6). As a result, the maximum inward traction stress (vector component perpendicular to the cell edge) was significantly reduced from 1,440 ± 35.44 pN/μm^2 to 1,180 ± 37.02 pN/μm^2 (Figure 4D), and even more strikingly the overall inward traction was lost (average traction stress; Figure 4E). It is noteworthy that the maximum pillar displacement values remained unchanged (data not shown), suggesting that there was a loss of organization but not of force production in absence of FHOD1.

The fact that the traction forces were present only as short bursts that changed magnitude and direction quickly indicated that myosins were pulling from multiple directions (see working model in Figure 5A). As a result, the forces were not directed and ultimately canceled each other out (Figures 4C and 4E). Expected consequences of this finding were a reduction in the retrograde flow and more off-axis movements. To test this prediction, we analyzed the retrograde flow by observing the behavior of fibronectin-coated beads (1 μm diameter) that were placed at the cell edge with the help of an optical trap (Choquet et al., 1997). Indeed, in FHOD1 knockdown cells, beads were transported inward at an overall slower pace and with many random off-axis movements (Figures 5B–5D; Movie S7).

FHOD1 knockdown cells on RGD-supported membranes also reduced actin polymerization from RGD-integrin clusters, as well as reduced cluster growth. There was no, or only slow, active actin polymerization or expansion outward from the clusters in FHOD1 knockdown cells (Figures 6A and 6B; Movie S8). RGD clusters frequently had no overlapping Lifeact signal (such as indicated by red arrows in Figure 6A), and the Lifeact signal was also detected in areas where no RGD clustering was detected (yellow arrows in Figure 6A). Furthermore, plotting of the average radial profiles and quantification of the integrated density over a radius of 2.5 μm from the centers of the clusters showed a significant decrease of the Lifeact and RGD fluorescence intensity (Figures 6C–6E). Thus, the knockdown of FHOD1 inhibited actin assembly from early integrin clusters and further impaired cluster maturation.

Together, these results indicated that FHOD1 was recruited to early integrin clusters downstream of receptor-ligand clustering, but independent of force. Furthermore, it was instrumental in organizing the actin for efficient force coupling at the adhesions and thus facilitated continued cluster growth.

FHOD1 Interaction with SFKs Is Necessary for Its Activation

Recent findings showed that the SFK inhibitor PP2 inhibited actin polymerization from early integrin clusters (Yu et al., 2011). Moreover, it was shown that FHOD1 was regulated downstream of SFKs, since treatment with the Src inhibitor PP2 abolished the FHOD1-induced transcription of the skeletal actin promoter (Koka et al., 2005). If FHOD1 played a role in the actin organization at integrin clusters, SFKs were possibly involved in the targeting of FHOD1 to integrin sites. Therefore, we analyzed targeting of FHOD1 to RGD-integrin clusters in PP2-treated fibroblasts. As reported previously (Yu et al., 2011), the PP2 treatment reduced growth of the integrin clusters. Furthermore, no ribbon-like polymerization of actin was detected and enrichment of FHOD1 around the clusters was reduced (Figure S6).

FHOD1 contains a conserved YEEI sequence on its N terminus (^{99}YEEI) that, when phosphorylated, constitutes a strong Src homology 2 (domain) (SH2) binding motif (Songyang et al., 1993; Figure 7A). Additionally, the poly-proline stretch of the FH1 domain is a putative SH3 binding site (Jia et al., 2005; Roskoski, 2004). Indeed, we confirmed tyrosine phosphorylation of immunoprecipitated full-length FHOD1, which was absent in a tyrosine to phenylalanine mutant (Y99F) and also lost after deletion of the poly-proline region (Δpoly-Pro; Figure 7B). Furthermore, SFKs coprecipitated with FHOD1, but the binding was reduced in case of the Y99F mutation and absent in the case of the Δpoly-proline mutation. Moreover, both mutations led to a loss of FHOD1 activity, as measured by Thr1141 phosphorylation, thus indicating that the interaction with SFKs via the poly-proline region resulted in tyrosine (Y99) phosphorylation, stronger SFK binding, and downstream activation of FHOD1.

To further investigate the interaction with SFKs, we used mouse fibroblast cells deficient in Src, Yes, and Fyn (SYF cells; Klinghoffer et al., 1999), as well as SYF cells that had Src reintroduced by retroviral transduction or that were stably transfected with either Yes or Fyn. Interestingly, coprecipitation of the SFKs and partial restoration of tyrosine and Thr1141 phosphorylation were detected with all three kinases, but only Src restored the phosphorylation to the control levels (Figure 7C). However, due to the retroviral transduction, as opposed to the stable transfection, Src levels exceeded those of the other kinases.

If SFKs were upstream of FHOD1 activation, knockdown of FHOD1 should not affect the spreading phenotype of SYF cells. In line with previous results (Cary et al., 2002; Klinghoffer et al., 1999; Kostic and Sheetz, 2006; von Wichert et al., 2003), SYF cells showed aberrant spreading behavior and reduced adhesion formation. Thus, the cells exhibited several similarities with FHOD1 knockdown cells, such as reduced cell area (Figures 7D and 7E), segmented cell morphology (Figure 7F), reduced adhesion area, and an increased number of small adhesions after 30 min of spreading (<0.2 μm^2; Figure 7G). FHOD1 knockdown in SYF cells, however, did not result in an aggravation of any of the spreading defects, indicating that FHOD1 was downstream of SFKs.

Targeting to Adhesion Sites Is Controlled by SFKs

Because both the Y99F and the Δpoly-Pro lacked Thr1141 phosphorylation (and hence were inactive) and FHOD1 binding to RGD clusters was reduced after PP2 treatment, we

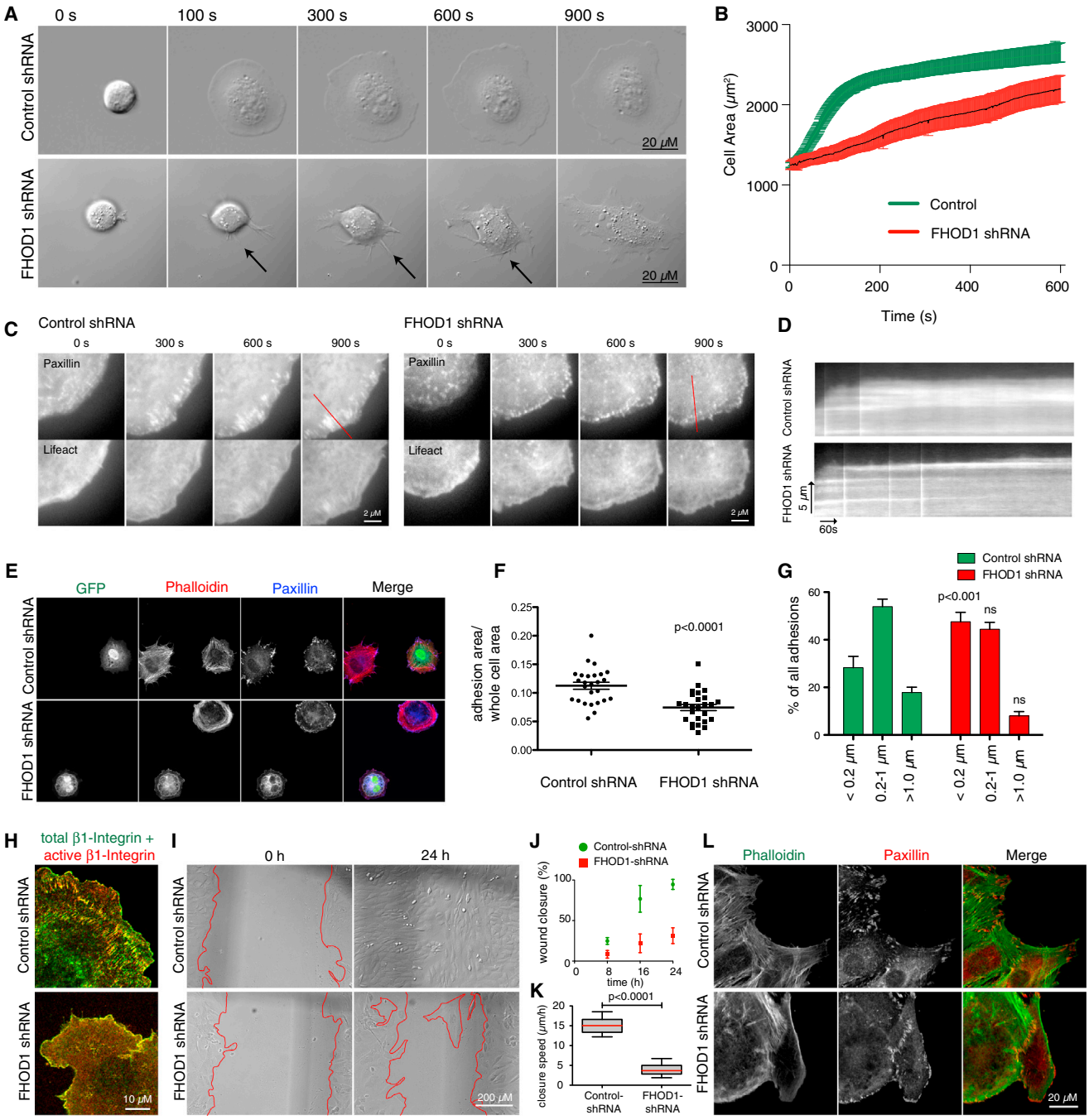

Figure 3. FHOD1 Knockdown Disrupts Cell Spreading

(A and B) FHOD1 knockdown cells spread more slowly. (A) MEF cells were transfected with control shRNA (upper panel) or FHOD1 shRNA plasmids (lower panels) for 72 hr, plated on fibronectin-coated coverslips, identified for knockdown by means of their GFP fluorescence, and imaged with a DIC microscope in intervals of 1 s. Arrows indicate a collapsing protrusion in a knockdown cell. (B) Spread area was determined with ImageJ and is shown as the average over n = 10 cells; error bars indicate SE; nonlinear regression and comparison between the fitted curves suggests a significant difference with $p < 0.0001$.

(C and D) MEF cells were transfected with control shRNA (upper panel) or FHOD1 shRNA plasmids. After 72 hr, cells were additionally transfected with paxillin-GFP and pRuby-Lifeact and imaged by TIRF microscopy in intervals of 3 s. Whereas most nascent adhesions mature to focal adhesions (see (D) for the kymographs of the regions marked by the red lines in (C)), the nascent adhesions in the knockdown cells do not mature and remain small adhesions that eventually turn over.

(E) Immunostaining of cells after 30 min spreading confirms a reduced adhesion area and adhesion maturation in FHOD1 knockdown cells.

(F) Quantification of the adhesion area as fraction of the whole cell area; n = 26 for both conditions.

(G) The decreased adhesion area is a result of reduced adhesion maturation. Single adhesions (n = 2,072 and n = 1,158 from ten control and FHOD1 shRNA-transfected cells, respectively) were measured with ImageJ and grouped into three categories (<0.2 μm^2, 0.2–1 μm^2, and >1 μm^2; error bars: SEM). FHOD1 knockdown cells have a significantly higher number of nascent (<0.2 μm^2) adhesions (two-way ANOVA and Bonferroni posttest: $p < 0.001$).

(legend continued on next page)

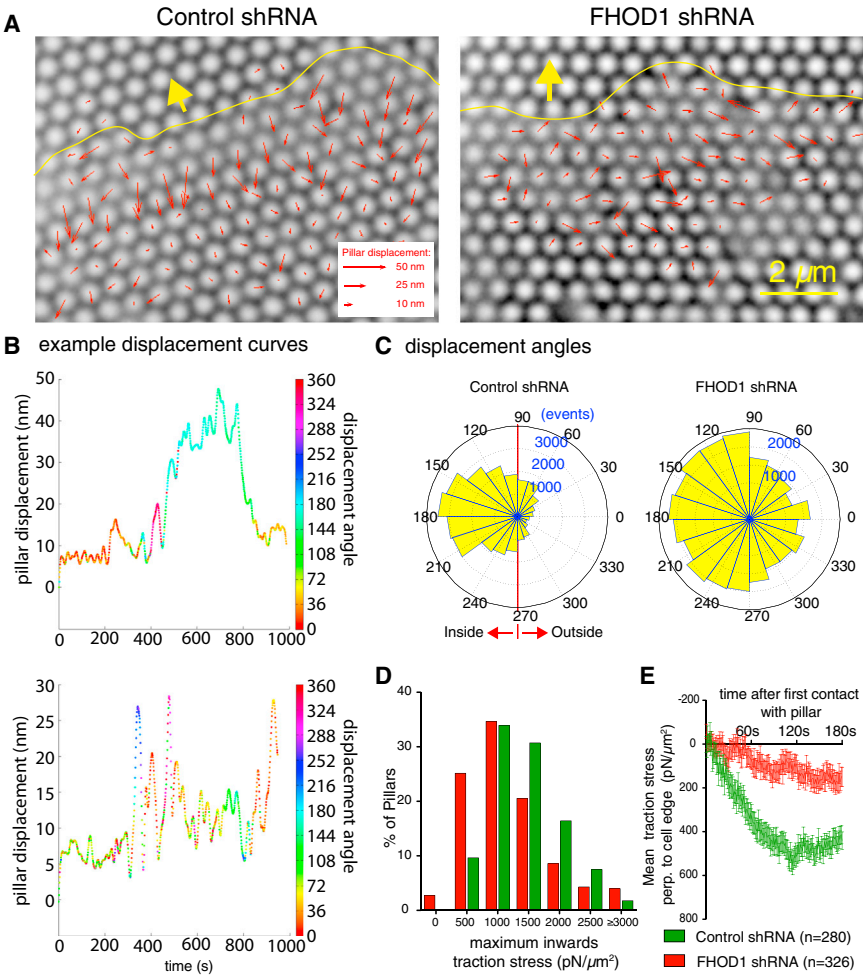

Figure 4. FHOD1 Knockdown Abolishes Inward-Directed Traction Stress

Control shRNA and FHOD1-shRNA-transfected cells were plated on PDMS pillar arrays (d = 0.5 μm; h = 1.1 μm) and imaged on a bright field microscope for ≥15 min, from the initiation of spreading, with one frame per second.

(A) Force maps indicate a loss of directed inward traction after FHOD1 knockdown. Red arrows, pillar displacements; yellow line, cell edge; yellow arrows, protrusion direction.

(B–E) Angle and magnitude of pillar displacements fluctuate in FHOD1 knockdown cells (see example curves with color-coded displacement angles in B), and pillar displacement angles are widely distributed (C). As a result, the maximum inward stress per pillar is reduced as well ($p < 0.0001$) (D) and there is a striking loss of the overall mean inward stress (E). The two data sets are statistically different (nonlinear regression and comparison of fits: $p < 0.0001$). In (C)–(E), n = 280 and 326 pillars from five cells each for the control and the FHOD1 knockdown, respectively. Displacement angles are all displacements over noise level (i.e., 10 nm) for 3 min after first contact with the cell edge (control, n = 35,196 events; FHOD1-shRNA, n = 36,872 events).

hypothesized that the interaction with SFKs was necessary for correct targeting to the integrins and subsequent activation by ROCK. Indeed, the typical localization pattern of FHOD1 with paxillin was lost in the SYF cells and was partially restored in all three SYF add-back cell lines (Figure 8A). Also, localization of the Y99F mutant to the adhesions was reduced and no overlap between FHOD1-Δpoly-Pro-GFP and paxillin was found (Figures 8B and 8D), whereas a constitutive inactive mutant of the ROCK phosphorylation sites (FHOD1-3A) still localized to the adhesions. Colocalization with actin decreased both with FHOD1-3A and with the Δpoly-proline mutation, which was presumably due to a loss of actin filaments in these cells (Figures 8C and 8E). Indeed, transfection with FHOD1-Δpoly-Pro-GFP induced a phenotype similar to a FHOD1 knockdown. Cells were depleted of actin filaments and lacked strong adhesions. In lipid bilayer experiments, the Δpoly-Pro mutant inhibited spreading entirely in ~40% of the cells. In the remaining cells, only small amounts of FHOD1 Δpoly-Pro were found around the RGD clusters and the clusters lacked the typical ribbon-like actin polymerization (Figures 8F–8I), indicating that the poly-proline deletion mutant sequestered endogenous FHOD1 away from the RGD clusters. Similarly, FHOD1-Y99F localization to the clusters was reduced and no Lifeact enrichment was found around the clusters. FHOD1-3A, in contrast, showed no targeting defect to the RGD clusters and actin enrichment was only slightly reduced (Figures 8H and 8I, not significant), indicating that this mutant did not display a dominant phenotype.

Together, the data indicated that SFKs bound to the FHOD1 poly-proline region, which resulted in phosphorylation of the YEEI motif and increased interaction with Src kinases. These events were necessary for the correct targeting of FHOD1 to integrins and its activation, which enabled actin polymerization from integrin clusters during cell spreading and migration.

DISCUSSION

In the present study, we combine the supported lipid bilayer system with high-resolution, force-sensing pillar arrays and

(H) Integrin activation at the cell edge is not affected by the FHOD1 knockdown. Green, total β1-integrin (12G10); red, activated β1-Integrin (9EG7).

(I) FHOD1-shRNA cells are closing wounds more slowly.

(J) Percentage of initial wound. Error bars = SEM.

(K) Speed of wound closure in μm/hr. Error bars: range, n = 10

(L) FHOD1 knockdown cells are forming only small adhesions at the cell edge during wound closure. Cells were fixed after 8 hr and stained for paxillin and F-actin. See also Figure S3 for the siRNA rescue and Figures S4 and S5 for the effects of the formin inhibitor smiFH2 on cell spreading and adhesion maturation, respectively.

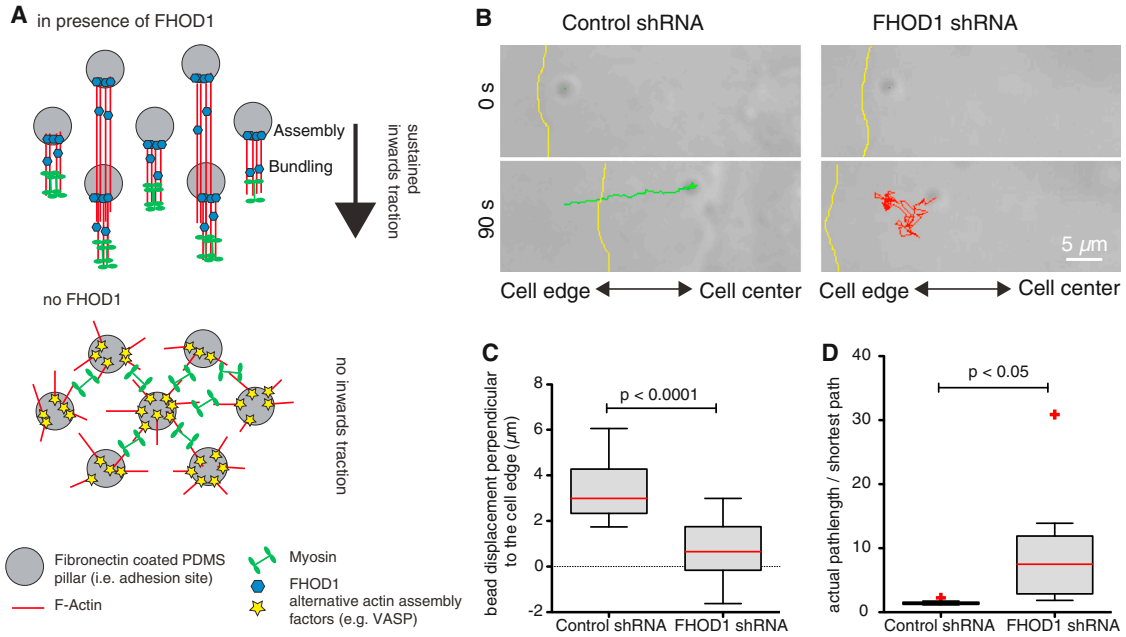

Figure 5. FHOD1 Knockdown Impairs the Retrograde Flow

(A) Working model: FHOD1 assembles actin filaments from integrin adhesion sites (e.g., pillar tops that are coated with fibronectin) and partially moves with the polymerizing actin to bundle the filaments into higher ordered structures. Myosin pulling is directed, resulting in inward traction and retrograde flow. In the absence of FHOD1, actin filaments are still formed by alternative actin assembly proteins such as VASP or ARP2/3, but to lesser extent. Also, the filaments lack organization, allowing the myosins to pull from multiple directions, thus cancelling out the forces and retrograde flow.

(B–D) Displacement analysis of fibronectin-coated beads (1 μm diameter) shows a reduced retrograde flow (C) and strongly increased off-axis movement (D) after 90 s (because of the fast displacements in control cells, inward movement stopped after ~90 s in some cases), thus supporting the working model. In (C) and (D), n = 10, p values from Student's t test, error bars indicate 1.5 × interquartile range (whiskers) with outliers displayed separately. Note that the cell edge retraction in the control shRNA cell (B) is the result of a typical retraction/protrusion cycle that started ~50 s after the imaging (see also Movie S7).

well-established cell spreading and migration assays on solid substrates to study actin assembly from early integrin clusters and subsequent adhesion formation. Importantly, since supported bilayers provide an environment in which there is no in-plane resistance to movement and thus provide an important contrast to planar glass substrates (Yu et al., 2011), we are able to characterize steps during adhesion formation that are prior to myosin activity. Sub-micron elastomer pillars, on the other hand, allow us to analyze localized traction stress with high precision. Using these methods, we show here that the formin family protein FHOD1 is critical for actin assembly from integrin clusters, inward-directed traction stress, as well as cell spreading and adhesion maturation. This is consistent with the hypothesis that the early spreading involves actin polymerization from ligand-bound integrin clusters to enable myosin-dependent cluster growth and further spreading through lamellipodial extension (Yu et al., 2011).

Furthermore, our results show that FHOD1 is required to form actin structures that allow effective coupling of myosin traction forces to the adhesion. Without FHOD1, forces on adhesion sites are present only as short bursts and not directed. Since there are other actin assembly proteins present at adhesions (e.g., VASP; Worth et al., 2010) or close to adhesions (e.g., ARP2/3), actin filaments are still formed in the absence of FHOD1, albeit to lower extents. However, without FHOD1 there is a lack of actin organization. This is in agreement with an actin bundling function, which was reported previously (Schönichen et al., 2013). Indeed, in lipid bilayer experiments, a part of the GFP-tagged FHOD1 moved outward from the integrin clusters, together with the polymerizing actin. Moreover, we also detected FHOD1 in a periodic pattern on fibronectin-coated glass, which could further indicate such bundling activity.

While the in vitro work by Schönichen et al. (2013) found that FHOD1 lacks actin nucleation activity and only displays weak filament elongation activity, other studies reported that FHOD1 enhanced actin polymerization in cyto (Gasteier et al., 2003, 2005; Koka et al., 2005; Watanabe et al., 1999), suggesting that FHOD1 might elongate previously nucleated filaments. Similarly, some of our results—especially the decreased actin polymerization from early integrin clusters in FHOD1 knockdown cells or in presence of the Δpoly-Pro or the Y99F mutant—clearly point toward an active actin elongation by FHOD1 during early spreading.

Independent of a bundling or elongation activity, our data show clearly that FHOD1 is targeted to integrin adhesions downstream of SFKs. Subsequently, it appears to be activated by ROCK to enable actin assembly from integrin clusters and cell spreading. This is in support of the proposed model that formin localization and activation are separate phenomena (Ramalingam et al., 2010).

Although it has been shown previously that FHOD1 is activated by ROCK (Hannemann et al., 2008; Schulte et al., 2008; Takeya et al., 2008) and regulated downstream of SFKs (Koka et al., 2005), details of the mechanism remained unclear. We

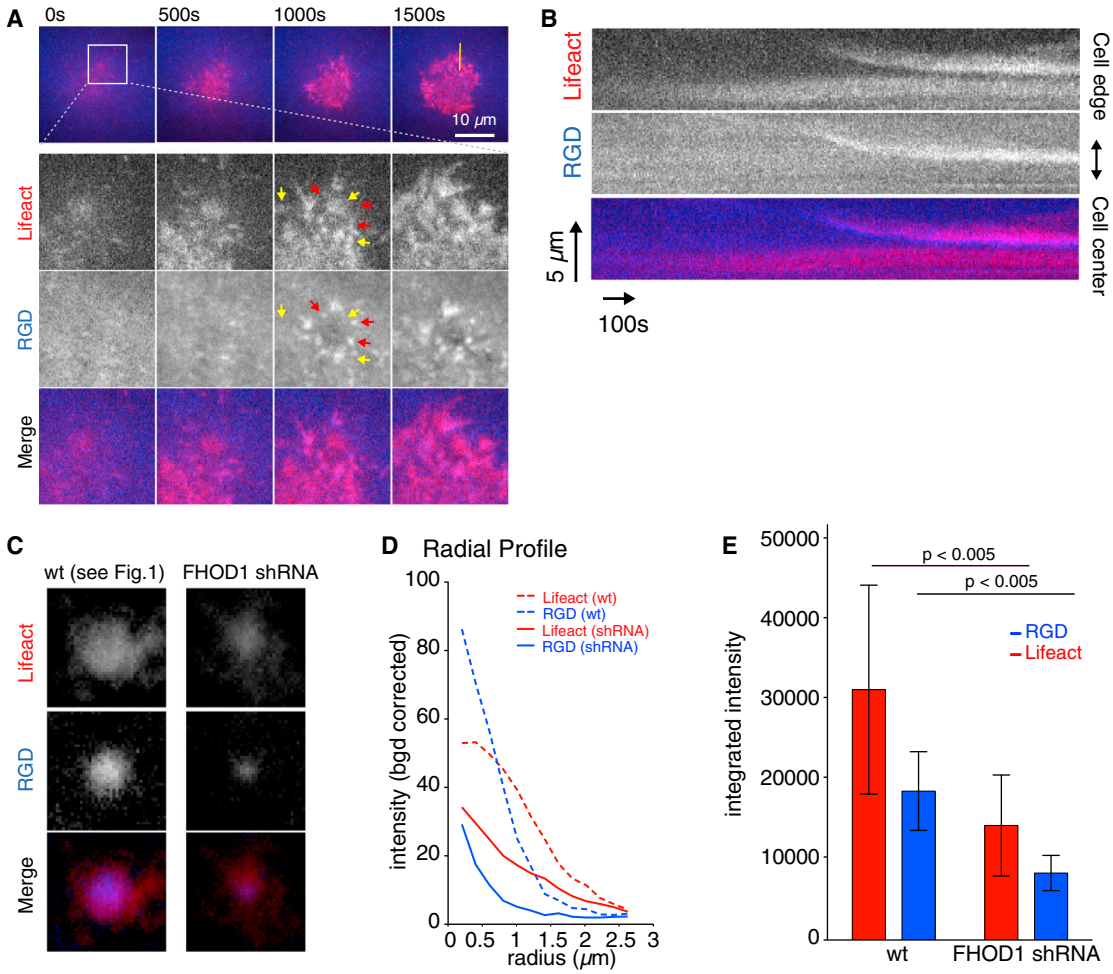

Figure 6. FHOD1 Knockdown Disrupts Actin Assembly from Integrin Clusters and Cluster Growth on Lipid Bilayer

(A) MEFs were transfected with FHOD1 shRNA and Ruby-Lifeact and plated on RGD-supported membrane. Due to the small size of the RGD clusters, a Kalman filter (ImageJ) was applied to the RGD channel. Red arrows indicate RGD clusters without actin, and yellow arrows show actin accumulations outside of RGD clusters.

(B) Kymograph of the region marked by a yellow line in (A).

(C and D) Averaging of the RGD clusters suggests reduced cluster size and F-actin around the RGD clusters (images of the average over 31 wild-type (WT; see also Figure 1) and 47 FHOD1 shRNA clusters are shown in (C) and the radial profiles are shown in (D).

(E) The integrated intensity of a ROI with a radius of 2.5 μm was measured with ImageJ. The graph shows the average and error bars show the SD over n = 7 cells for both conditions. Student's t tests confirm a significant reduction in both F-actin and RGD levels around the cluster center.

confirm here that the activation is downstream of SFKs in several ways: (1) abolishing the interaction by incubation with PP2, (2) using SYF cells, or (3) mutation of the interaction sites all reduce activation of FHOD1. In contrast, a constitutive inactive mutant (FHOD1-3A; Takeya et al., 2008) can still localize to the adhesion regions. Furthermore, binding of Src to the poly-proline region, followed by phosphorylation of a YEEI sequence on the N terminus, enables the subsequent activation. FH1-SH3 domain interactions have been reported previously for yeast and trematode formins (Kamei et al., 1998; Quack et al., 2009), and a similar mechanism has been detected also for other proteins, such as p130Cas, where the interaction between the poly-proline region and the Src SH3 domain serves to activate Src and results in subsequent phosphorylation of p130Cas (Bibbins et al., 1993; Pellicena and Miller, 2001; Pellicena et al., 1998). The interaction with SFKs might bring FHOD1 in close proximity to ROCK at the membrane (Riento and Ridley, 2003) and thus enable the activation. During cell spreading, this results in a peak of FHOD1 activity at a time when the majority of cells form new adhesions all around the cell edge. At later time points during spreading (and also migration) nascent adhesions are formed as well, but only a small portion of the edge moves out at any time (not all around the cell edge and in a large fraction of the spreading cells). Therefore, FHOD1 phosphorylation returns to the baseline levels in spread cells. Rapid and transient phosphorylation of FHOD1 after receptor engagement was also found in other cell types, i.e., after collagen-related peptide stimulation in human platelets (Thomas et al., 2011) and could mark a universal event in the stimulation of actin polymerization upon integrin clustering.

Our results show that only Src can efficiently phosphorylate FHOD1 at Y99 to enable the downstream activation by

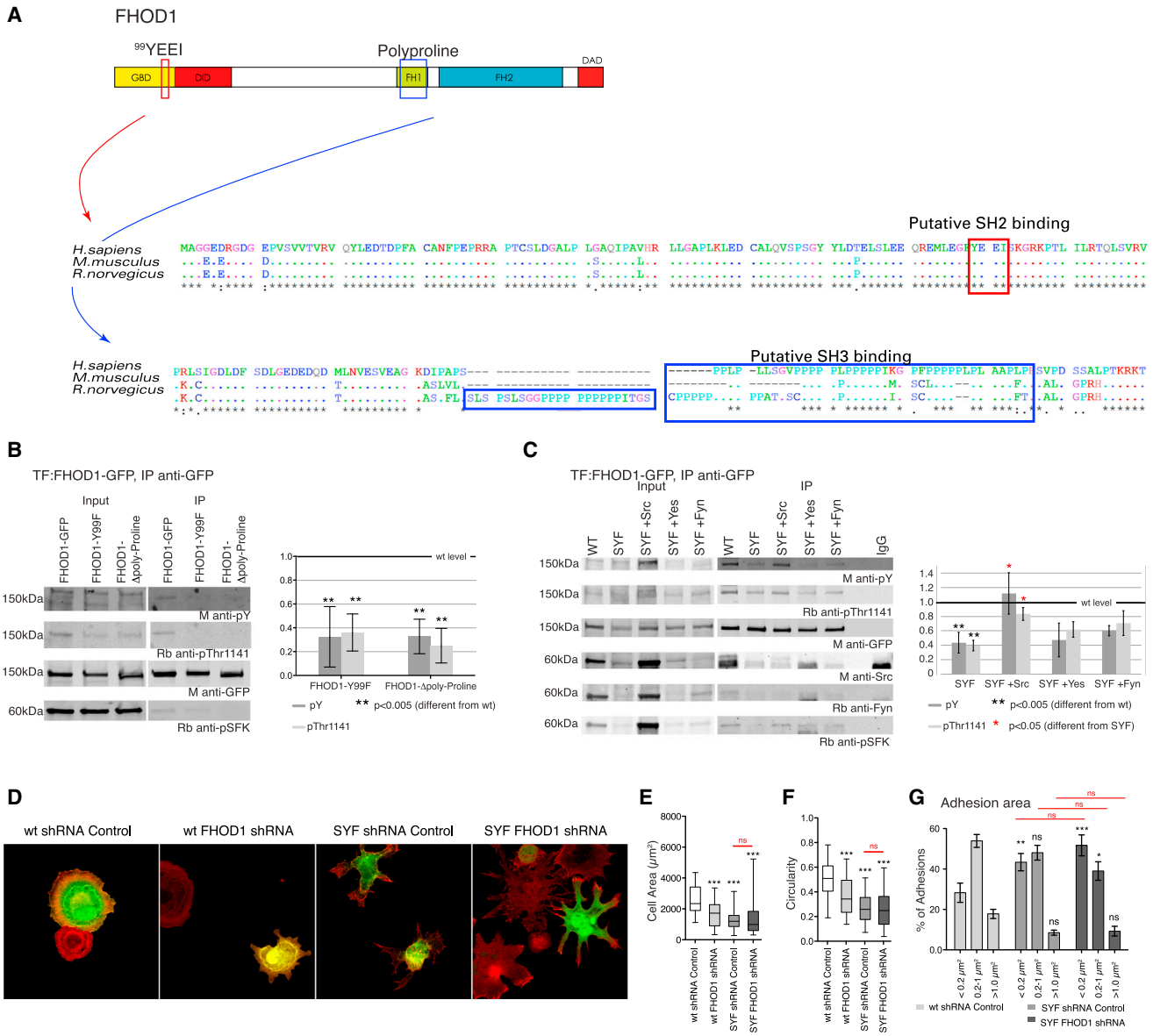

Figure 7. FHOD1 Is Phosphorylated by SFKs

(A) Schematic of FHOD1 and the putative SH2 and SH3 binding sites and alignment of human (*H. sapiens*), mouse (*M. musculus*), and rat (*R. norvegicus*) FHOD1 sequences.

(B) Immunoprecipitated wild-type FHOD1, but not the Y99F or the poly-proline deletion (FHOD1-Δpoly-proline) construct, shows a band when probed with an anti-phospho-tyrosine antibody. Similarly, a band with the phospho-Thr1141 antibody can be detected only on wild-type FHOD1, and interaction with SFKs (anti-pSFK) is reduced or abolished for FHOD1-Y99F and FHOD1-Δpoly-proline, respectively. n = 3, error bars indicate SD.

(C) Tyrosine phosphorylation and Thr1141 phosphorylation are reduced in SYF cells, but can be restored by Src; n = 3, error bars indicate SD. Incubation with Src, Fyn, or pSFK antibodies suggests interaction with Src, Yes, and Fyn.

(D–G) SYF cells spread more slowly (D and E) and have irregular cell shapes (D and F). However, the phenotype is not aggravated by FHOD1 knockdown (error bars: range). Similarly, SYF cells have a reduced adhesion area and more immature adhesions after 30 min spreading (G), irrespective of FHOD1 levels. For p values from Student's t test (E and F) or two-way ANOVA with Bonferroni posttests (G): error bars, SEM; *$p < 0.05$, **$p < 0.005$, ***$p < 0.001$; ns, not significant. Results from t tests between SYF shRNA control and SYF FHOD1 shRNA are shown in red.

See also Figure S6 for PP2 treatment.

ROCK. However, in Yes and Fyn add-back cells, the expression levels of the respective SFKs are lower than in wild-type cells and thus the SFK activity might not be sufficient for a full recovery of FHOD1 phosphorylation on a cellular level, but rather only lead to localized effects. Indeed, our results suggest that add back of Yes or Fyn is sufficient to restore the targeting at least partially. Nevertheless, we cannot exclude that these effects on adhesion targeting are only due to a redundancy between the SFKs (Lowell and Soriano, 1996).

Together, our study shows that FHOD1 is a critical actin assembly factor at the early integrin clusters during cell spreading and migration, and it triggers a cascade of events that eventually produces longer term adhesions through the polymerization and bundling of actin filaments. Although several formins that were previously studied in fibroblasts participate in adhesion formation and/or maturation (Goode and Eck, 2007; Gupton et al., 2007; Yamana et al., 2006), our study shows specific targeting of a formin to integrin adhesions. Furthermore, our data show that this targeting depends on integrin-ligand engagement, but not myosin contractility. This could be important since recent findings have highlighted the role of mammalian and yeast formins as mechanosensors (Courtemanche et al., 2013; Higashida et al., 2013; Jégou et al., 2013). In these studies, formin activity was enhanced in presence of profilin by a pulling force on tethered mDia1 or Bni1p in flow chambers and on membrane-bound mDia1 in cells. Although it remains to be seen if the same applies to FHOD1, a force-dependent regulation of an adhesion-localized actin assembly factor would provide a direct link between integrin mechanosensing and actin-driven cell protrusion.

EXPERIMENTAL PROCEDURES

Cell Culture and Transfections

RPTP$\alpha^{+/+}$ mouse embryonic fibroblast (MEF) cells and SYF cells were cultured in Dulbecco's modified Eagle's medium (DMEM) with 10% fetal bovine serum and 1% penicillin/streptomycin to 70%–80% confluency and passaged the day before the experiment. If not indicated otherwise, cells were transfected for 24 hr with an AMAXA nucleofector using the MEF transfection KIT (Lonza) according to the manufacturer's instructions. SYF+Src cells were obtained from ATCC; SYF+Fyn and SYF+Yes add-back cells were a kind gift from Dr. Yasuhiro Sawada.

Microscopy

Differential interference contrast (DIC) microscopy and bright field time-lapse imaging were performed with an Olympus IX-70 inverted microscope maintained at 37°C using a 100× numerical aperture (N.A.) 1.40, 60× N.A. 1.40, or a 20× N.A. 0.80 oil objective (all Olympus), a CoolSNAP HQ charge-coupled device (CCD) camera (Photometrics), and micro-manager or MetaMorph microscopy software (Molecular Devices).

Total internal reflection fluorescence (TIRF) images and time-lapse micrographs were taken using an Olympus IX81 fluorescence microscope maintained at 37°C with a 60× N.A. 1.45 objective and a Cool Snap FX cooled CCD camera (Photometrics) controlled by SimplePCI software (Compix). Confocal microscopy was performed on a Zeiss LSM700 laser-scanning confocal microscope using a 63× N.A. 1.40 objective (Zeiss) or an Olympus Fluoview FV500 laser-scanning confocal microscope using a 60× N.A. 1.40 objective (Olympus).

Spreading Assays

Cells were spread on human plasma full-length pure fibronectin-coated (10 μg/ml; Roche) silanized cover glasses or, for western blotting and immunoprecipitation assays, on fibronectin-coated tissue culture dishes. Cells were trypsinized, washed with soybean trypsin inhibitor, centrifuged, and preincubated in Ringer medium (150 mM NaCl, 5 mM KCl, 1 mM $CaCl_2$, 1 mM $MgCl_2$, 20 mM HEPES, and 2 g/L D-Glucose at pH 7.4) for 30 min prior to the experiment. Cells were plated and imaged by time-lapse microscopy (DIC or TIRF), or fixed with 4% paraformaldehyde/PBS and stained for confocal microscopy. For western blotting and coimmunoprecipitation assays, cells were lysed in 20 mM Tris, 137 mM NaCl, 10% glycerol, and 1% NP40 at pH 8.0, including protease and phosphatase inhibitor cocktails (cOmplete EDTA-free Protease Inhibitor Cocktail Tablets and PhosSTOP Phosphatase Inhibitor Cocktail Tablets, both Roche) on ice, snap frozen, rethawed, and cleared from cell debris by centrifugation. In case of smiFH2 (Sigma), blebbistatin (Sigma), or Y-27632 (Tocris) treatment, indicated doses of drugs were present during the preincubation as well as the spreading experiment. For FHOD1-GFP immunoprecipitations, we used the Crosslink immunoprecipitation kit (Pierce) and monoclonal mouse anti-GFP antibody (Roche).

Analysis of Edge Velocities

Spread area was calculated with the "Analyze Particles" function of ImageJ, after using the "Find Edges" function and thresholding to binarize the cells. Where necessary, "Close," "Fill Holes," and "Remove Outliers" functions were used to receive a coherent mask of the cell. Outlines of the measured cells were added to the original image series with the "Image Calculator" function as a control. Spread phases were identified after plotting the logarithm of the area versus the logarithm of the time (Dubin-Thaler et al., 2008; see also Figure S1A). Average edge velocities were calculated as the slope of the radius of a circle with the measured cell area over the time.

Wound Healing Assays

Cells were transfected with FHOD1 shRNA or Control shRNA plasmids and cultured for 96 hr in the presence of 150 μg/ml zeozin. Subsequently, cells were plated to confluency on fibronectin-coated tissue culture, or if intended for immunofluorescence, on fibronectin-coated glass-bottom dishes (MatTek). After 12 hr, a wound was applied with a pipette tip, cells were washed twice with fresh full medium, and marked areas were imaged every 8 hr with an Olympus IX81 fluorescence microscope maintained at 37°C with a 10× N.A. 0.3 objective (Olympus). The (paxillin) adhesion area was measured with ImageJ within a 50 μm wide region of interest (ROI), after thresholding and using the "Analyze Particle" function. Regions with a strong, diffuse cytoplasmic paxillin signal were excluded from the analysis.

Traction Force Measurements

Pillar arrays (1.1 μm in height, 0.5 μm diameter, 1 μm center to center, k = 13.9 nN/μm) coated with 10 μg/ml of fibronectin (Invitrogen) were prepared as described previously (Ghassemi et al., 2012). Briefly, cells were spread on pillar arrays and bright field movies were taken as described above with a frame rate of one frame per second. Displacements were measured with ImageJ, using the NanoTracking plugin.

Bead Displacement Analysis

Silica microspheres 1 μm in diameter (Bangs Laboratories) were activated with cyanogen bromide and covalently labeled with fibronectin according to the manufacturer's instructions (TechNote 205). Cells (Control and FHOD1 shRNA transfected for 4 days) and beads were added onto fibronectin-coated coverslips. Beads were placed at the edges of cells with an optical trap, using a 2 W diode pumped 1,064 nm laser (CrystalLaser) until they were fixed on the cell surface (i.e., the optical trap force was unable to produce a detectable movement of the bead) and visualized with a 100× N.A. 1.3 objective on an inverted Axiovert 100 TV microscope, equipped with Nomarsky optics. After thresholding, beads were tracked with ImageJ (Fiji) using the MTrack2 plugin.

Functionalized Supported Lipid Bilayer Membrane

RGD peptide, a biotinylated peptide of cyclo (Arg-Gly-Asp-D-Phe-Lys(biotin-polyethylene glycol-polyethylene glycol)), was purchased from Peptides International (3697-PI). Both 1,2-dioleoyl-sn-glycero-3-phosphocholine (DOPC) and 1,2-dipalmitoyl-sn-glycero-3-phosphoethanolamine-N-(cap biotinyl) (16:0 biotinyl-Cap-PE) were purchased from Avanti Polar Lipids. Cascade Blue neutravidin was purchased from Invitrogen. Detailed preparation methods were previously described (Yu et al., 2011). In brief, small lipid vesicles (0.4 mol% of biotinyl-Cap-PE and 99.6 mol% of DOPC) were made by sonication and then were used to deposit onto glass cover glass under aqueous condition with 150 mM PBS in room temperature. Neutravidin serves as the link between biotinyl-Cap-PE and biotinylated RGD peptide. A total of 1 μg/mL of fluorescently labeled neutravidin (Cascade Blue) was added onto supported lipid membranes for 30 min incubation. After washing off excess neutravidin, 1 μg/mL of biotinylated RGD was added to neutravidin-coated supported membranes for another 30 min. Excess RGD was removed by serial solvent exchange, 25 mL of 150 mM PBS in each chamber, and then 15 mL of serum-free DMEM. In general, the 2D diffusion coefficient of RGD-supported membrane is measured as high as 2.5 $\mu m^2/s$.

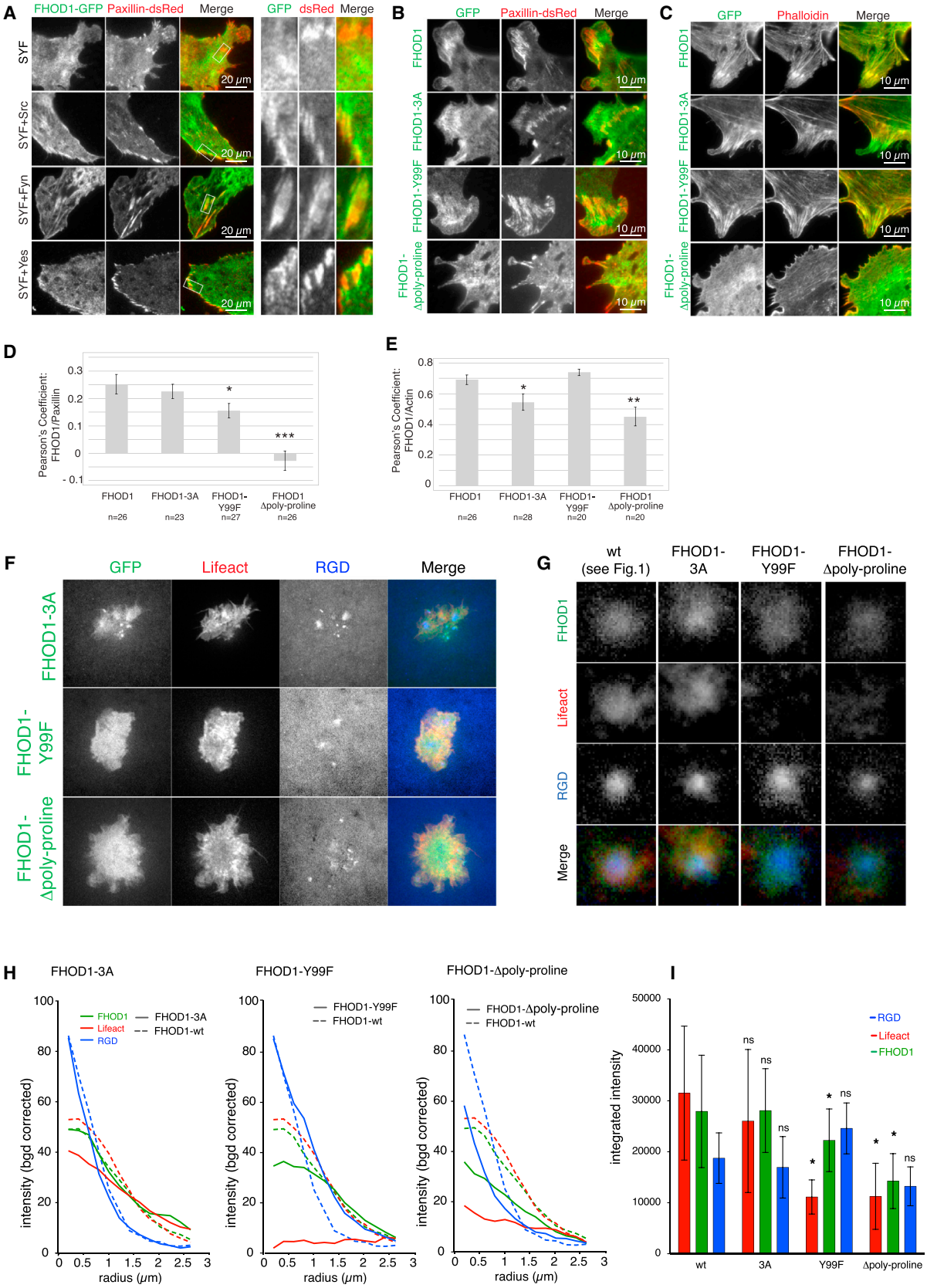

(legend on next page)

RGD Cluster Analysis

A tiff stack of RGD clusters from cells that were spread for 5 min was created and the average image calculated with ImageJ. A circular ROI with a radius of 2.5 μm was drawn around the center of the clusters. To analyze the enrichment of proteins around the clusters, we subtracted the average pixel intensity outside the ROI from each channel. The resulting image was used to quantify the integrated intensity of each channel and create radial profiles with ImageJ, using the Radial Profile Plot plugin. The data are presented as the radial profile of the average over all clusters for a certain condition, as well as the mean integrated intensities (±SD) of the average clusters from single cell.

Immunofluorescence

Immunofluorescence staining was carried out as described previously (Iskratsch et al., 2010). Briefly, fixed cells were permeabilized with 0.2% Triton X-100 in PBS for 5 min, or 0.02% Triton for 5 min for the integrin staining, blocked with MAXblock blocking medium (Active Motif) according to the manufacturer's instructions, and stained with the primary antibody mix in immunostaining buffer (1% BSA, 20 mM Tris-base, 155 mM NaCl, 2 mM EGTA, and 2 mM $MgCl_2$, pH 7.5) for 1 hr under shaking at room temperature. Cells were washed three times with PBS and incubated with the secondary antibody mix, containing Phalloidin (Alexa Fluor 546 or Alexa Fluor 633-Phalloidin; Invitrogen) where indicated. After washing three times with PBS, cells were mounted in 0.1 M Tris-HCl/glycerol (3:7) and 50 mg/ml N-propyl-gallate, pH 9.5.

Statistical Testing

In the current study, two-tailed Student's t test was used for comparison between two groups. Data sets were tested for normal distribution using the Shapiro-Wilk test. If not stated otherwise, all box plots are displayed as median (central line), upper and lower quartile (box), ±1.5 × interquartile range (whiskers), with outliers displayed separately. Two-way ANOVA and Bonferroni posttests were calculated with Graphpad Prism 5.

Image Processing

Original digital images obtained were assembled to the figures and labeled using InDesign or Illustrator (Adobe). Only linear contrast adjustments were used and were always applied to the entire image.

Supplemental Experimental Procedures

Additional experimental procedures can be found in the Supplemental Experimental Procedures, including the antibodies, sequences of the siRNAs, and primers used in this work.

SUPPLEMENTAL INFORMATION

Supplemental Information includes Supplemental Experimental Procedures, six figures, and eight movies and can be found with this article online at http://dx.doi.org/10.1016/j.devcel.2013.11.003.

ACKNOWLEDGMENTS

We are grateful to Yasuhiro Sawada for the SYF add-back cell lines. We also thank Reuven Agami for providing pSUPER, Anne Ridley for FMNL3, Arthur Alberts for mDia2, Roland Wedlich-Söldner for Lifeact, and Michael Partridge for the paxillin plasmids. We gratefully acknowledge the help of Lale Alpar and the critical reading and helpful comments provided by Nicolas Biais and Haguy Wolfenson. This work was supported by an American Heart Association fellowship (to T.I.) and NIH grants EB001480 and EY016586.

Received: August 1, 2013
Revised: October 19, 2013
Accepted: November 4, 2013
Published: December 9, 2013

REFERENCES

Alexandrova, A.Y., Arnold, K., Schaub, S., Vasiliev, J.M., Meister, J.J., Bershadsky, A.D., and Verkhovsky, A.B. (2008). Comparative dynamics of retrograde actin flow and focal adhesions: formation of nascent adhesions triggers transition from fast to slow flow. PLoS ONE *3*, e3234.

Bibbins, K.B., Boeuf, H., and Varmus, H.E. (1993). Binding of the Src SH2 domain to phosphopeptides is determined by residues in both the SH2 domain and the phosphopeptides. Mol. Cell. Biol. *13*, 7278–7287.

Cai, Y., Rossier, O., Gauthier, N.C., Biais, N., Fardin, M.A., Zhang, X., Miller, L.W., Ladoux, B., Cornish, V.W., and Sheetz, M.P. (2010). Cytoskeletal coherence requires myosin-IIA contractility. J. Cell Sci. *123*, 413–423.

Campellone, K.G., and Welch, M.D. (2010). A nucleator arms race: cellular control of actin assembly. Nat. Rev. Mol. Cell Biol. *11*, 237–251.

Cary, L.A., Klinghoffer, R.A., Sachsenmaier, C., and Cooper, J.A. (2002). SRC catalytic but not scaffolding function is needed for integrin-regulated tyrosine phosphorylation, cell migration, and cell spreading. Mol. Cell. Biol. *22*, 2427–2440.

Choi, C.K., Vicente-Manzanares, M., Zareno, J., Whitmore, L.A., Mogilner, A., and Horwitz, A.R. (2008). Actin and alpha-actinin orchestrate the assembly and maturation of nascent adhesions in a myosin II motor-independent manner. Nat. Cell Biol. *10*, 1039–1050.

Choquet, D., Felsenfeld, D.P., and Sheetz, M.P. (1997). Extracellular matrix rigidity causes strengthening of integrin-cytoskeleton linkages. Cell *88*, 39–48.

Courtemanche, N., Lee, J.Y., Pollard, T.D., and Greene, E.C. (2013). Tension modulates actin filament polymerization mediated by formin and profilin. Proc. Natl. Acad. Sci. USA *110*, 9752–9757.

Di Nardo, A., Cicchetti, G., Falet, H., Hartwig, J.H., Stossel, T.P., and Kwiatkowski, D.J. (2005). Arp2/3 complex-deficient mouse fibroblasts are viable and have normal leading-edge actin structure and function. Proc. Natl. Acad. Sci. USA *102*, 16263–16268.

Döbereiner, H.G., Dubin-Thaler, B.J., Hofman, J.M., Xenias, H.S., Sims, T.N., Giannone, G., Dustin, M.L., Wiggins, C.H., and Sheetz, M.P. (2006). Lateral membrane waves constitute a universal dynamic pattern of motile cells. Phys. Rev. Lett. *97*, 038102.

Dubin-Thaler, B.J., Hofman, J.M., Cai, Y., Xenias, H., Spielman, I., Shneidman, A.V., David, L.A., Döbereiner, H.G., Wiggins, C.H., and Sheetz, M.P. (2008). Quantification of cell edge velocities and traction forces reveals distinct motility modules during cell spreading. PLoS ONE *3*, e3735.

Gasteier, J.E., Madrid, R., Krautkrämer, E., Schröder, S., Muranyi, W., Benichou, S., and Fackler, O.T. (2003). Activation of the Rac-binding partner FHOD1 induces actin stress fibers via a ROCK-dependent mechanism. J. Biol. Chem. *278*, 38902–38912.

Figure 8. FHOD1 Is Recruited to Adhesions Downstream of SFKs

(A) FHOD1 localization to adhesions is lost in SYF cells, but can be restored by the reintroduction of Src, Yes, or Fyn. SYF cells or add-back cells for the indicated kinase were cotransfected with FHOD1-GFP and paxillin-dsRed and imaged by TIRF microscopy.

(B and D) TIRF microscopy shows localization of WT-FHOD1, constitutive inactive FHOD1 (FHOD1-3A), and the Y99F mutant, but not FHOD1-Δpoly-proline to the adhesion region (B). Quantification of colocalization shown in (D).

(C and E) All FHOD1 constructs localized to actin filaments (C), but with FHOD1-3A or FHOD1-Δpoly-proline the correlation was reduced (E).

(F–I) Wild-type FHOD1 and constitutive inactive FHOD1-3A, but not FHOD1-Y99F or FHOD1-Δpoly-proline localize to RGD clusters; representative images of cells that were spread on the bilayers for 5 min. Average over RGD clusters (after 5 min spreading) of cells transfected with the indicated constructs (G). Radial profile of the average clusters (H) and the average integrated intensity (I) (error bars indicate SD) of clusters of single cells (n = 7 cells for WT, 5 cells for FHOD1-3A and FHOD1-Δpoly-proline and 4 cells for FHOD1-Y99F).

Gasteier, J.E., Schroeder, S., Muranyi, W., Madrid, R., Benichou, S., and Fackler, O.T. (2005). FHOD1 coordinates actin filament and microtubule alignment to mediate cell elongation. Exp. Cell Res. *306*, 192–202.

Ghassemi, S., Meacci, G., Liu, S., Gondarenko, A.A., Mathur, A., Roca-Cusachs, P., Sheetz, M.P., and Hone, J. (2012). Cells test substrate rigidity by local contractions on submicrometer pillars. Proc. Natl. Acad. Sci. USA *109*, 5328–5333.

Giannone, G., Dubin-Thaler, B.J., Döbereiner, H.G., Kieffer, N., Bresnick, A.R., and Sheetz, M.P. (2004). Periodic lamellipodial contractions correlate with rearward actin waves. Cell *116*, 431–443.

Giannone, G., Dubin-Thaler, B.J., Rossier, O., Cai, Y., Chaga, O., Jiang, G., Beaver, W., Döbereiner, H.G., Freund, Y., Borisy, G., and Sheetz, M.P. (2007). Lamellipodial actin mechanically links myosin activity with adhesion-site formation. Cell *128*, 561–575.

Goley, E.D., and Welch, M.D. (2006). The ARP2/3 complex: an actin nucleator comes of age. Nat. Rev. Mol. Cell Biol. *7*, 713–726.

Goode, B.L., and Eck, M.J. (2007). Mechanism and function of formins in the control of actin assembly. Annu. Rev. Biochem. *76*, 593–627.

Gupton, S.L., Eisenmann, K., Alberts, A.S., and Waterman-Storer, C.M. (2007). mDia2 regulates actin and focal adhesion dynamics and organization in the lamella for efficient epithelial cell migration. J. Cell Sci. *120*, 3475–3487.

Hannemann, S., Madrid, R., Stastna, J., Kitzing, T., Gasteier, J., Schönichen, A., Bouchet, J., Jimenez, A., Geyer, M., Grosse, R., et al. (2008). The Diaphanous-related Formin FHOD1 associates with ROCK1 and promotes Src-dependent plasma membrane blebbing. J. Biol. Chem. *283*, 27891–27903.

Higashida, C., Kiuchi, T., Akiba, Y., Mizuno, H., Maruoka, M., Narumiya, S., Mizuno, K., and Watanabe, N. (2013). F- and G-actin homeostasis regulates mechanosensitive actin nucleation by formins. Nat. Cell Biol. *15*, 395–405.

Huveneers, S., and Danen, E.H. (2009). Adhesion signaling - crosstalk between integrins, Src and Rho. J. Cell Sci. *122*, 1059–1069.

Iskratsch, T., Lange, S., Dwyer, J., Kho, A.L., dos Remedios, C., and Ehler, E. (2010). Formin follows function: a muscle-specific isoform of FHOD3 is regulated by CK2 phosphorylation and promotes myofibril maintenance. J. Cell Biol. *191*, 1159–1172.

Iskratsch, T., Reijntjes, S., Dwyer, J., Toselli, P., Dégano, I.R., Dominguez, I., and Ehler, E. (2013). Two distinct phosphorylation events govern the function of muscle FHOD3. Cell. Mol. Life Sci. *70*, 893–908.

Jégou, A., Carlier, M.F., and Romet-Lemonne, G. (2013). Formin mDia1 senses and generates mechanical forces on actin filaments. Nat. Commun. *4*, 1883.

Jia, C.Y., Nie, J., Wu, C., Li, C., and Li, S.S. (2005). Novel Src homology 3 domain-binding motifs identified from proteomic screen of a Pro-rich region. Mol. Cell. Proteomics *4*, 1155–1166.

Jiang, G., Giannone, G., Critchley, D.R., Fukumoto, E., and Sheetz, M.P. (2003). Two-piconewton slip bond between fibronectin and the cytoskeleton depends on talin. Nature *424*, 334–337.

Kamei, T., Tanaka, K., Hihara, T., Umikawa, M., Imamura, H., Kikyo, M., Ozaki, K., and Takai, Y. (1998). Interaction of Bnr1p with a novel Src homology 3 domain-containing Hof1p. Implication in cytokinesis in Saccharomyces cerevisiae. J. Biol. Chem. *273*, 28341–28345.

Klinghoffer, R.A., Sachsenmaier, C., Cooper, J.A., and Soriano, P. (1999). Src family kinases are required for integrin but not PDGFR signal transduction. EMBO J. *18*, 2459–2471.

Koka, S., Minick, G.T., Zhou, Y., Westendorf, J.J., and Boehm, M.B. (2005). Src regulates the activity of the mammalian formin protein FHOD1. Biochem. Biophys. Res. Commun. *336*, 1285–1291.

Kostic, A., and Sheetz, M.P. (2006). Fibronectin rigidity response through Fyn and p130Cas recruitment to the leading edge. Mol. Biol. Cell *17*, 2684–2695.

Lai, F.P., Szczodrak, M., Block, J., Faix, J., Breitsprecher, D., Mannherz, H.G., Stradal, T.E., Dunn, G.A., Small, J.V., and Rottner, K. (2008). Arp2/3 complex interactions and actin network turnover in lamellipodia. EMBO J. *27*, 982–992.

Lowell, C.A., and Soriano, P. (1996). Knockouts of Src-family kinases: stiff bones, wimpy T cells, and bad memories. Genes Dev. *10*, 1845–1857.

Mellor, H. (2010). The role of formins in filopodia formation. Biochim. Biophys. Acta *1803*, 191–200.

Nolen, B.J., Tomasevic, N., Russell, A., Pierce, D.W., Jia, Z., McCormick, C.D., Hartman, J., Sakowicz, R., and Pollard, T.D. (2009). Characterization of two classes of small molecule inhibitors of Arp2/3 complex. Nature *460*, 1031–1034.

Pellicena, P., and Miller, W.T. (2001). Processive phosphorylation of p130Cas by Src depends on SH3-polyproline interactions. J. Biol. Chem. *276*, 28190–28196.

Pellicena, P., Stowell, K.R., and Miller, W.T. (1998). Enhanced phosphorylation of Src family kinase substrates containing SH2 domain binding sites. J. Biol. Chem. *273*, 15325–15328.

Quack, T., Knobloch, J., Beckmann, S., Vicogne, J., Dissous, C., and Grevelding, C.G. (2009). The formin-homology protein SmDia interacts with the Src kinase SmTK and the GTPase SmRho1 in the gonads of Schistosoma mansoni. PLoS ONE *4*, e6998.

Ramalingam, N., Zhao, H., Breitsprecher, D., Lappalainen, P., Faix, J., and Schleicher, M. (2010). Phospholipids regulate localization and activity of mDia1 formin. Eur. J. Cell Biol. *89*, 723–732.

Riento, K., and Ridley, A.J. (2003). Rocks: multifunctional kinases in cell behaviour. Nat. Rev. Mol. Cell Biol. *4*, 446–456.

Roca-Cusachs, P., Iskratsch, T., and Sheetz, M.P. (2012). Finding the weakest link: exploring integrin-mediated mechanical molecular pathways. J. Cell Sci. *125*, 3025–3038.

Roca-Cusachs, P., del Rio, A., Puklin-Faucher, E., Gauthier, N.C., Biais, N., and Sheetz, M.P. (2013). Integrin-dependent force transmission to the extracellular matrix by α-actinin triggers adhesion maturation. Proc. Natl. Acad. Sci. USA *110*, E1361–E1370.

Roskoski, R., Jr. (2004). Src protein-tyrosine kinase structure and regulation. Biochem. Biophys. Res. Commun. *324*, 1155–1164.

Schönichen, A., Mannherz, H.G., Behrmann, E., Mazur, A.J., Kühn, S., Silván, U., Schoenenberger, C.A., Fackler, O.T., Raunser, S., Dehmelt, L., and Geyer, M. (2013). FHOD1 is a combined actin filament capping and bundling factor that selectively associates with actin arcs and stress fibers. J. Cell Sci. *126*, 1891–1901.

Schulte, A., Stolp, B., Schönichen, A., Pylypenko, O., Rak, A., Fackler, O.T., and Geyer, M. (2008). The human formin FHOD1 contains a bipartite structure of FH3 and GTPase-binding domains required for activation. Structure *16*, 1313–1323.

Songyang, Z., Shoelson, S.E., Chaudhuri, M., Gish, G., Pawson, T., Haser, W.G., King, F., Roberts, T., Ratnofsky, S., Lechleider, R.J., et al. (1993). SH2 domains recognize specific phosphopeptide sequences. Cell *72*, 767–778.

Steffen, A., Faix, J., Resch, G.P., Linkner, J., Wehland, J., Small, J.V., Rottner, K., and Stradal, T.E. (2006). Filopodia formation in the absence of functional WAVE- and Arp2/3-complexes. Mol. Biol. Cell *17*, 2581–2591.

Svitkina, T.M., and Borisy, G.G. (1999). Arp2/3 complex and actin depolymerizing factor/cofilin in dendritic organization and treadmilling of actin filament array in lamellipodia. J. Cell Biol. *145*, 1009–1026.

Takeya, R., Taniguchi, K., Narumiya, S., and Sumimoto, H. (2008). The mammalian formin FHOD1 is activated through phosphorylation by ROCK and mediates thrombin-induced stress fibre formation in endothelial cells. EMBO J. *27*, 618–628.

Thomas, S.G., Calaminus, S.D., Machesky, L.M., Alberts, A.S., and Watson, S.P. (2011). G-protein coupled and ITAM receptor regulation of the formin FHOD1 through Rho kinase in platelets. J. Thromb. Haemost. *9*, 1648–1651.

von Wichert, G., Jiang, G., Kostic, A., De Vos, K., Sap, J., and Sheetz, M.P. (2003). RPTP-alpha acts as a transducer of mechanical force on alphav/beta3-integrin-cytoskeleton linkages. J. Cell Biol. *161*, 143–153.

Watanabe, N., Kato, T., Fujita, A., Ishizaki, T., and Narumiya, S. (1999). Cooperation between mDia1 and ROCK in Rho-induced actin reorganization. Nat. Cell Biol. *1*, 136–143.

Worth, D.C., Hodivala-Dilke, K., Robinson, S.D., King, S.J., Morton, P.E., Gertler, F.B., Humphries, M.J., and Parsons, M. (2010). Alpha v beta3 integrin spatially regulates VASP and RIAM to control adhesion dynamics and migration. J. Cell Biol. *189*, 369–383.

Yamana, N., Arakawa, Y., Nishino, T., Kurokawa, K., Tanji, M., Itoh, R.E., Monypenny, J., Ishizaki, T., Bito, H., Nozaki, K., et al. (2006). The Rho-mDia1 pathway regulates cell polarity and focal adhesion turnover in migrating cells through mobilizing Apc and c-Src. Mol. Cell. Biol. *26*, 6844–6858.

Yu, C.H., Law, J.B., Suryana, M., Low, H.Y., and Sheetz, M.P. (2011). Early integrin binding to Arg-Gly-Asp peptide activates actin polymerization and contractile movement that stimulates outward translocation. Proc. Natl. Acad. Sci. USA *108*, 20585–20590.